Phase Reconstruction of the Polycrystalline Structure of Internal Organs Tissues in the Differentiation of Alcohol and Carbon Monoxide Poisoning

Ya. Ivashkevich[1], O. Wanchulyak[1], V. Bachinsky[1], Yu. Tomka[2], I. Soltys[2], O. Dubolazov[2], V. Dvorjak[2]

[1] Bukovinian State Medical University, 3 Theatral Sq., Chernivtsi, Ukraine, 58000
[2] Chernivtsi National University, 2 Kotsiubynskyi Str., Chernivtsi, Ukraine, 58012

a.dubolazov@chnu.edu.ua

ABSTRACT

Our paper are presented the results of forensic medical differential investigations of cases of alcohol and carbon monoxide poisoning using the methods of differential Mueller-matrix polarization-phase tomography For this method we used multichannel sensing of different-polarized laser beams of brain histological sections.

Keywords: tomography, phase reconstruction, alcohol and carbon monoxide poisoning, diagnostics.

1. Introduction

1.1. Biological layer model

The principles of our model analysis of the processes of formation of parameters of microscopic images of biological layers of tissues and fluids of human organs are based on the well-known Muller-matrix polarimetric analytical approach[1-5]. According to this approach, a biological object is considered as a two-component ("isotropic-anisotropic") structural matrix, - Fig. 1**.**

Biological layer		
Polycrystalline silicon component		Amorphous component
Linear (LB) and circular (CB) birefringence		Absorption
2nd, 3rd and 4th parameters of the Stokes vector		1st parameter of the Stokes vector
Mueller matrix invariants (MMI) of phase anisotropy		Mueller matrix invariants of absorption
Information Parameters		
MMI LB	MMI CB	MMI absorption

Fig. 1. Polarization model of an optically thin histological section of biological tissue

The development of such analytical ideas was the latest results on optical modeling of a more general and widespread class of biological objects with partial depolarization, which are theoretically presented in [6,7] and experimentally developed in [1,4-6,8-13]. The scheme of such optical modeling of the structure of biological layers is illustrated in Fig. 2

Biological layer			
Polarization component		Depolarization (diffuse) component	
Average values of linear (LB) and circular (CB) birefringence		Fluctuations in the magnitude of linear (FLB) and circular (FCB) birefringence	
1st order differential matrix elements		2nd order differential matrix elements	
Polarization-phase tomograms of phase anisotropy		Diffuse tomograms of phase anisotropy	
LB Maps	CB Maps	FLB Maps	FCB Maps

Fig. 2. Polarization model of an optically thick (diffuse) histological section of biological tissue

Here is the structural and logical diagram and design of forensic medical research using the method of polarization-phase tomography of the polycrystalline structure of histological sections of tissues of internal organs and a polycrystalline film of blood from coronary heart disease (CHD), as well as cases of poisoning with alcohol and carbon monoxide, - Fig. 3.

Method			
Polarization-phase tomography of the polycrystalline component of biological preparations of human internal organs			
Parameters			
Tomograms of coordinate distributions of average values of linear birefringence (LB) of polycrystalline networks of biological preparations of human internal organs			
The object			
Histological sections of internal organs			
Control group 1 (CHD)	Control group 2 (alcohol poisoning)		Control group 3 (carbon monoxide poisoning)
Data analysis			
statistical approach			
Average, *Sr* LB	Dispersion, *Dp* LB	Asymmetry, *As* LB	Excess, *Ek* LB
Інформаційний підхід			
Sensitivity, *Se*	Specificity, *Sp*		Accuracy, *Ac*
Forensic medical criteria for polarization-phase tomographic differentiation of cases of poisoning with alcohol and carbon monoxide			

Fig. 3. The structural-logical diagram of differential Mueller-matrix polarization-phase tomography of the polycrystalline component of biological preparations

2. Methods of polarization-phase tomography of biological layers

In our investigations we used next algorithm[5]

1	Source of optical sensing	Gas helium-neon laser; Wavelength 0.6328 μm; Power 10 mW
2	Optical probe spatial structure forming unit	Optical collimator for forming a parallel laser beam with a cross section of 5 mm
3	Multichannel unit for forming the polarization structure of the optical probe	System for forming linear (0^0;90^0;45^0) and right-circular polarization (linear polarizer (Achromatic True Zero-Order Waveplate) - a quarter-wave plate (B + W Kaesemann XS-

		Pro Polarizer MRC Nano)).
4	Object block	Microscopic coordinate node
5	Microscopic image forming unit	Polarized microobjectives (Nikon CFI Achromat P, working distance – 30mm, focal distance - 50mm, NA – 0.1, magnification – 4x)
6	Multi-channel polarization filtering unit	Transmission system of linearly (0^0;90^0;45^0;135^0) and right- and left-circularly polarized components
7	Digital microscopic image sampling and flotation unit	Digital CCD camera (The Imaging Source DMK 41AU02.AS, monochrome 1/2 "CCD, Sony ICX205AL (progressive scan); resolution - 1280x960, size light-sensitive area - 7600x6200mkm; sensitivity - 0.05 lx, dynamic range - 8 bit, SNR - 9 bit) by polarization microobjective 7 (Nikon CFI Achromat P, focal length - 30 mm, numerical aperture - 0.1 increase - 4x)
8	Stokes polarimetry computer data processing unit	Calculation algorithms: - magnitudes of linear birefringence of fibrillar networks; - values of circular birefringence of molecular complexes; - statistical moments of the 1st - 4th orders

Fig. 4. Structural and logical scheme of the method of polarization-phase tomography of biological layers

Examples of the implementation of polarization reconstruction (tomography) of the distributions of the average values of the birefringence value of the polycrystalline component of the samples of histological sections of biological tissues are presented in Fig.5 and Fig. 6

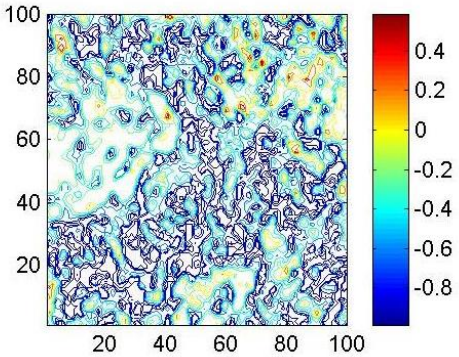

Fig. 5. Map of linear birefringence of histological section of the brain of a deceased due to coronary heart disease

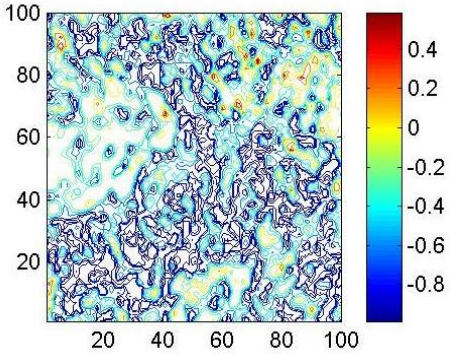

Fig. 6. Map of circular birefringence of the histological section of the brain of the deceased due to coronary heart disease

2. Results and discussion

On the fragments of Fig. 7 are shown tomograms (fragments (1) - (3)) of the distribution of the LB value of histological sections of the brain from the research (fragments (1)) and two control (fragments (2), (3)) groups of samples.

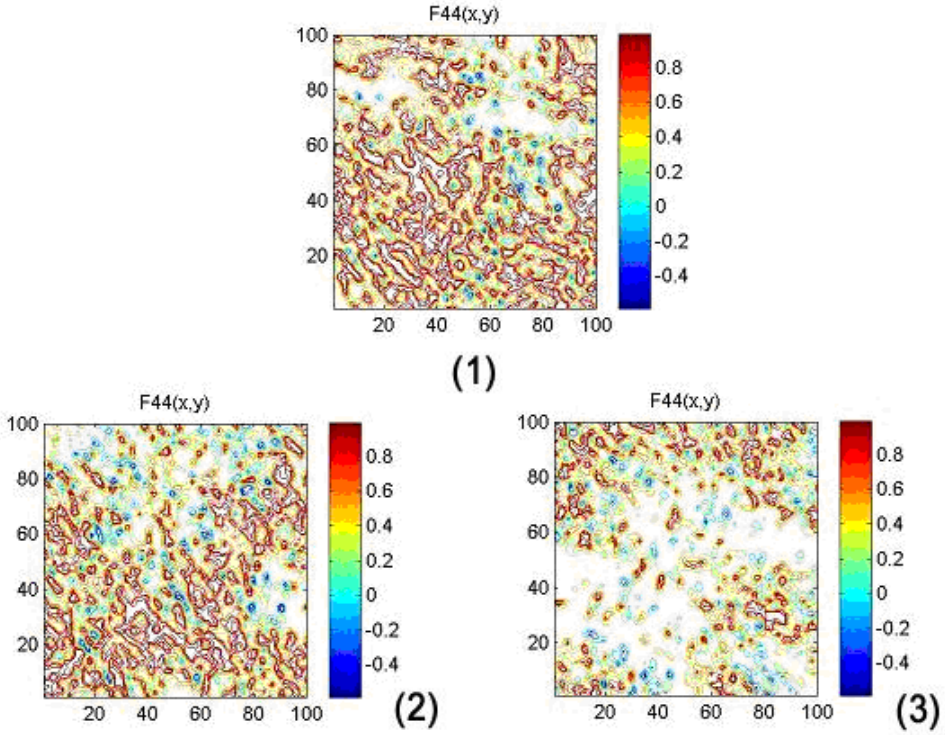

Fig. 7. Tomograms of coordinate distributions of the magnitude of the linear birefringence of histological sections of the brain

Significant differences were found in the topographic structure of the tomograms of LB histological sections of the brain of patients who died from coronary heart disease and poisoning with alcohol and carbon monoxide.
Quantitatively, such a process is accompanied by a decrease in the average and dispersion values, as well as an increase in the values of statistical moments of the 3rd and 4th orders characterizing the distribution of the LB value of the samples of histological sections of the brain of the dead as a result of poisoning with alcohol and carbon monoxide, table 1.

Table 1. Value of the samples of histological sections of the brain of the dead as a result of poisoning with alcohol and carbon monoxide

Sample	Histological sections of the brain		
Statistical moments	Group 1 ($n=45$)	Group 2 ($n=45$)	Group 3 ($n=45$)
Average, Sr x10^{-2}	$0{,}59 \pm 0{,}027$	$0{,}41 \pm 0{,}023$	$0{,}25 \pm 0{,}012$
$p_1; p_2$,		p_1 p 0,05	p_2 p 0,05
$p_{1;2}$		$p_{1;2}$ π 0,05	
Dispersion, Dp x10^{-2}	$0{,}49 \pm 0{,}025$	$0{,}29 \pm 0{,}014$	$0{,}15 \pm 0{,}007$
$p_1; p_2$,		p_1 π 0,05	p_2 π 0,05
$p_{1;2}$		$p_{1;2}$ p 0,05	
Asymmetry, As	$0{,}43 \pm 0{,}021$	$0{,}87 \pm 0{,}039$	$1{,}42 \pm 0{,}065$
$p_1; p_2$,		p_1 p 0,05	p_2 π 0,05
$p_{1;2}$		$p_{1;2}$ p 0,05	
Excess, Ek	$0{,}77 \pm 0{,}031$	$1{,}27 \pm 0{,}058$	$1{,}98 \pm 0{,}092$
$p_1; p_2$,		p_1 π 0,05	p_2 π 0,05
$p_{1;2}$		$p_{1;2}$ p 0,05	

The statistical reliability ($p_1; p_2; p_{1;2}$ p 0,05) of the use in forensic medical differentiation of samples of histological sections of the brain of deceased from all groups of the average Sr, dispersion Dp, asymmetry As and excess Ek, characterizing the polarized-reproduced coordinate distribution of the average LB value, has been established.
The results of an information analysis of the strength of the polarization-phase tomography method are presented in table 2.

Table. 2. Operational strength characteristics of the polarization-phase tomography method

Sample	Histological sections of the brain							
$St_{i=1.2.3.4}$	Average, Sr		Dispersion, Dp		Asymmetry, As		Excess, Ek	
Se,%	a=38; b=5	88.8	a=37; b=5	88,8	a=39; b=3	93,3	a=40; b=2	95,5
Sp,%	c=37; d=5	88,8	c=37; d=6	86,6	c=38; d=4	91,1	c=39; d=3	93,3
Ac,%	N=45	88,8	n=45	87,7	n=45	92,7	n=45	94,4

Conclusion

It was demonstrated good ($Sr, Dp \to 88\% - 89\%$) and excellent ($As, Ek \to 93\% - 95\%$) level of balanced accuracy of differential diagnosis of cases of alcohol and carbon monoxide poisoning by polarizing reconstruction of tomograms of linear birefringence of fibrillar networks of brain tissue.

References

[1]. Ushenko, O. G., Grytsyuk, M., Ushenko, V. O., Bodnar, G. B., Vanchulyak, O., & Meglinskiy, I. (2018, January). Differential 3D Mueller-matrix mapping of optically anisotropic depolarizing biological layers. In *Thirteenth International Conference on Correlation Optics* (Vol. 10612, p. 106121I). International Society for Optics and Photonics.

[2]. Y. Yasuno, M. Ju, Y. Hong, S. Makita, and M. Miura, "In Vivo Three-Dimensional Investigation of Tissue

Birefringence by Jones Matrix Tomography," in 2013 Conference on Lasers and Electro-Optics Pacific Rim, (Optical Society of America, 2013), paper WJ4_2.

[3]. Toshitaka Kobata and Takanori Nomura, "Digital holographic three-dimensional Mueller matrix imaging," Applied Optics Vol. 54, No. 17, pp.5591-5596 (2015).

[4]. Ushenko, A.G., Dubolazov, O.V., Bachynsky, V.T., Peresunko, A.P., Vanchulyak, O.Y., "On the feasibilities of using the wavelet analysis of mueller matrix images of biological crystals," (2010) Advances in Optical Technologies, 162832.

[5]. Zabolotna, N.I., Wojcik, W., Pavlov, S.V., Ushenko, O.G., Suleimenov, B., "Diagnostics of pathologically changed birefringent networks by means of phase Mueller matrix tomography," (2013) Proceedings of SPIE - The International Society for Optical Engineering, 8698, 86980.

[6]. Ushenko, A.G., "Correlation Processing and Wavelet Analysis of Polarization Images of Biological Tissues," (2001) Optics and Spectroscopy (English translation of Optika i Spektroskopiya), 91 (5), pp. 773-778.

[7]. Ushenko, A.G., Ermolenko, S.B., Burkovets, D.N., Ushenko, Yu.A., "Polarization microstructure of laser radiation scattered by optically active biotissues," (1999) Optika i Spektroskopiya, 87 (3), pp. 470-474.

[8]. Ushenko, A.G., Dubolazov, A.V., Ushenko, V.A., Novakovskaya, O.Y., "Statistical analysis of polarization-inhomogeneous Fourier spectra of laser radiation scattered by human skin in the tasks of differentiation of benign and malignant formations," (2016) Journal of Biomedical Optics, 21 (7), 071110.

[9]. Bekshaev AY, Angelsky OV, Sviridova SV, Zenkova CY. Mechanical action of inhomogeneously polarized optical fields and detection of the internal energy flows. Adv Opt Technol 2011.

[10]. Angelsky, O. V., Maksimyak, P. P., &Perun, T. O. (1993). Optical correlation method for measuring spatial complexity in optical fields. Optics Letters, 18(2), 90-92.

[11]. Angelsky, O. V., Bekshaev, A. Y. A., Maksimyak, P. P., Maksimyak, A. P., & Hanson, S. G. (2018). Low-temperature laser-stimulated controllable generation of micro-bubbles in a water suspension of absorptive colloid particles. Optics Express, 26(11), 13995-14009.

[12]. Angelsky, O. V. (2007). Optical correlation techniques and applications. Optical correlation techniques and applications (pp. 1-270).

[13]. Angelsky, O. V., Ushenko, A. G., Pishak, V. P., Burkovets, D. N., Yermolenko, S. B., Pishak, O. V., &Ushenko, Y. A. (2000). Coherent introscopy of phase-inhomogeneous surfaces and layers. Paper presented at the Proceedings of SPIE - the International Society for Optical Engineering, 4016 413-418.